

Influence of the Graded Index Cholesteric Liquid Crystal Reflectors on the Luminescent Solar Concentrator Efficiency

Ramin Zohrabi^{a,*}, Abdolrahman Namdar^a, Sohrab Ahmadi-Kandjani^a, and Babak Olyaeefar^b

^aFaculty of Physics, University of Tabriz, Tabriz, Iran

^bUNAM-Institute of Materials Science and Nanotechnology, Bilkent University, Ankara, Turkey

*Corresponding Author: r.zohrabi@tabrizu.ac.ir

Regular paper: Received: April. 09, 2023, Revised: Jun. 08, 2023, Accepted: Jun. 13, 2023,
Available Online: Jun. 15, 2023, DOI: 10.52547/ijop.16.2.211

ABSTRACT— This article examines the impact of graded-index reflectors (GIRs) constructed from cholesteric liquid crystals (CLCs) on the modification of escape-cone loss and the improvement of luminescent solar concentrator (LSC) efficiency. GIRs are comprised of a structure in which the refractive index changes gradually with a spatial function. In this study, the LSC is a planar optical waveguide made of Poly (methyl methacrylate) (PMMA) with dimensions of $5 \times 5 \times 0.5$ cm³ and contains $\text{CH}_3\text{NH}_3\text{PbBr}_3$ perovskite material as a fluorophore. Two types of GIRs are employed at the bottom of the LSC: periodic and quasi-periodic GIRs. Periodic reflectors (PRs) have a refractive index matrix that gradually changes with a periodic sinusoidal function, while the refractive index matrix of the quasi-periodic reflectors (QPRs) gradually changes with a chirped sinusoidal function. To analyze the models of the study, Monte-Carlo and Finite-Difference Time-Domain (FDTD) methods were utilized in conjunction with experimental results. The results indicated that the reflection band of a PR exhibited the maximum overlap (lowest escape cone) with the dye emission spectrum when the mirror's reflection band underwent a redshift of 20 nm compared to the dye emission spectrum. On the other hand, the QPR generated a broader reflection band, resulting in complete overlap and higher efficiency. Moreover, GIRs enhanced sunlight absorption in the LSC by reflecting transmitted solar photons through it. The optical efficiency (OE) of the LSC increased by 12% (33%) once a periodic (quasi-periodic) reflector is utilized. Furthermore, GIRs reduced escape cone loss, thereby increasing reabsorption, and subsequently, the system

selected a lower optimal concentration to minimize reabsorption losses.

KEYWORDS: Cholesteric liquid crystal, graded index reflector, luminescent solar concentrator, Monte-Carlo, Perovskite.

I. INTRODUCTION

Renewable energy sources offer cleaner and more efficient solutions for meeting our long-term energy needs, while also contributing to job creation and local economic development. Furthermore, investing in renewable energy can help mitigate the adverse effects of climate change by reducing greenhouse gas emissions and improving air quality. Consequently, governments are increasingly emphasizing on the utilization of renewable energy resources. Among these resources, solar energy stands out as a widely available option. Solar cells are highly efficient devices for converting solar energy into electrical energy, making them a favorable choice [1]. Concentrating sunlight onto solar cells can reduce the required panel area and lower investment costs in solar farms. Moreover, the use of rotating solar panel systems to track sunlight direction comes with additional expenses that can be mitigated through the implementation of direction-free concentrators. Additionally, residential areas often face challenges in achieving high efficiency with solar cells due to indirect and scattered sunlight, along with limited available installation space. Luminescent Solar

Concentrators (LSCs) offer a solution to these obstacles. An LSC, in essence, is a planar optical waveguide that incorporates fluorescent dye molecules. Its design provides a large-exposed area to sunlight and thin edges, allowing for easy and flexible attachment to solar cells. By absorbing solar photons and subsequently re-emitting them with a redshift, LSCs achieve a luminescent concentration of sunlight. The re-emitted light is guided to the edges through total internal reflection (TIR) [2], [3]. Re-emission occurring within the escape cone, where total internal reflection (TIR) cannot be achieved, represents a significant loss in LSCs. Extensive efforts have been made to mitigate this loss [4]. Graded-index reflectors (GIRs) based on cholesteric liquid crystals (CLCs) have emerged as promising tools for reducing escape cone losses [5]. These reflectors consist of anisotropic CLC molecules, which, due to anchoring forces, align in a stacked manner with a gradual rotation in their orientation. This arrangement creates a medium with a gradually changing refractive index. If the spatial frequency of this gradual rotation remains constant, it forms a periodic-gradual refractive index medium, known as a Bragg reflector. Depending on the period length and the angle of incident light, periodic reflectors (PRs) can reflect different regions of the optical spectrum [6]-[8]. Furthermore, the spatial rotation frequency of the CLC molecules can be chirped, resulting in a quasi-periodic reflector (QPR) with a modifiable reflection band. Various techniques can be employed to achieve chirped frequency rotations in CLCs [9]-[12]. By utilizing GIRs, it is possible to redirect the emitted light from dyes into the LSC, bypassing the limitations imposed by TIR. Building upon our group's pioneering work on perovskite-based LSCs [13-16], substantial efforts have been dedicated to enhancing their efficiency [17]-[20]. In the present study, it was attempted to investigate the influence of CLC-based periodic and quasi-periodic GIRs on LSCs incorporating $CH_3NH_3PbBr_3$ perovskite material as a fluorophore. For QPRs, a periodic function was employed with a linearly varying spatial frequency. To analyze the performance of present structures, Finite-Difference Time-

Domain (FDTD) [21], [22] and Monte Carlo [20], [23] simulation methods were utilized.

II. MODEL AND METHOD

The LSC under investigation is depicted in Fig. 1 (a). It comprises a smooth and transparent waveguide housing dye molecule, with a GIR positioned at the bottom, and solar cells located at the edges. The GIRs, composed of CLCs, possess a structure as illustrated in Fig. 1 (b). CLC molecules exhibit birefringence and possess an intrinsic dipole moment.

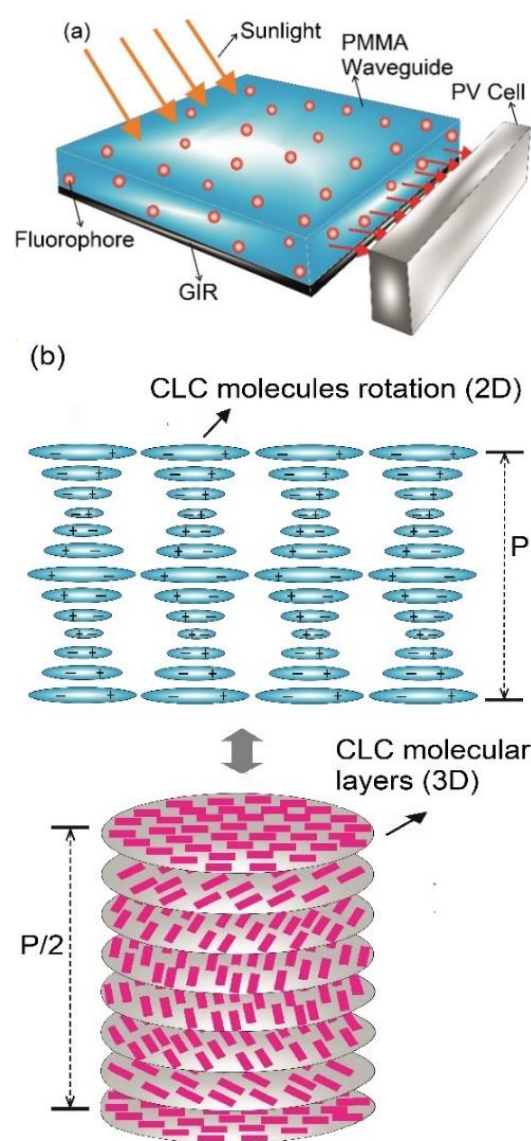


Fig. 1. Schematic representation of (a) Considered LSC structure containing PMMA waveguide (blue blade), dye molecules (red squares), GIR (black layer), and PV cell (grey blade). (b) Gradual rotation of the CLC molecules in 2D and 3D in a GIR.

Through the action of anchoring forces, the molecular layers are stacked with a gradual rotation around the axis perpendicular to the dipole vector (helix axis), resulting in a medium with a gradually changing refractive index. The extent of the rotation angle depends on the type and quantity of chiral material employed. Under conditions of homogeneous and stable synthesis, the rotation angle between the molecules remains consistent. After each full rotation of 360° , a pitch (p) of equal length is obtained. By repeating these pitches, a periodic medium akin to a Bragg reflector is formed. Through various techniques, it is possible to introduce a second-order gradient in the pitch length along the thickness of the reflector. This variation in pitch length gives rise to a QPR structure. These reflectors are quasi-periodic photonic crystals and can have a modified reflection band [24], [25].

The general spatial varying function of the RI is defined by the following relation [26], [27]:

$$n(z) = R_z(z) \begin{pmatrix} n_o & 0 & 0 \\ 0 & n_o & 0 \\ 0 & 0 & n_e \end{pmatrix} R_z^T(z), \quad (1)$$

where,

$$R(z) = \begin{pmatrix} \cos(\theta(z)) & -\sin(\theta(z)) & 0 \\ \sin(\theta(z)) & \cos(\theta(z)) & 0 \\ 0 & 0 & 1 \end{pmatrix}, \quad (2)$$

is the rotation matrix around the z-axis and $R_z^T(z)$ is its transpose matrix and θ is the rotation angle. Depending on the θ sign we have a right-handed or left-handed pitch rotation. $\theta(z)$ is defined as a following relation [28]:

$$\theta(z) = 2\pi \left[f_i z + \left(\frac{f_f - f_i}{2L} \right) z^2 \right] \quad (3)$$

In this regard, f_i and f_f are the initial and final spatial rotation frequencies respectively and define as pitches number per unit length (1/p). Depending on the value of the start and end frequencies, this equation shows a mirror with fixed or linearly variable pitch lengths along the z-axis. The relation between the reflection

wavelength and the length of the pitches can be expressed as [29]:

$$\lambda_c = n_{av} p (1 - n^2 \sin^2 \varphi)^{1/2} \quad (4)$$

where λ_c is the central reflection wavelength, n_{av} is the average refractive index of the host CLC, φ is the incidence angle, and n is the refractive index of the ambient medium. A mirror with a left (right) handed twist, completely reflects left (right) handed polarized incident light. And for un-polarized light, it reflects 50% of incident light [30].

The total efficiency of an LSC, μ_t , is [22], [30]:

$$\mu_t = \mu_g \mu_o, \quad (5)$$

where μ_g , geometric efficiency, and μ_o , optical efficiency (OE), are defined as $\frac{T}{A}$ and $\frac{N_{edge}}{N_{incident}}$, respectively, where T is the area of the edges attached to solar cells, A is the surface area exposed to incident sunlight, N_{edge} is the number of photons reaching the edges, and the number of sun photons incident on the LSC is given by N . Assuming the geometrical components are constant, the focus is on OE. It depends on the refractive index of the waveguide, dye concentration, dye absorption and emission spectrums, and the used mirrors. We employ a Monte Carlo method to determine the OE of the concentrator. This method is based on the probability distribution functions (PDFs): PDFs of the wavelength and direction of the sun's incident photons, absorption and re-emission of the dyes, and the reflection and transmission in the waveguide boundaries. PDF of the wavelength of the incident light is the Air mass 1.5, which is used as a reference distribution function in all articles for the comparability of research results in the field of solar cell efficiency. The direction of incident sunlight photons is a constant random function, therefore, all directions are equally possible. Additionally, our PDFs for reflection and transmission are based on Fresnel coefficients and the GIR reflection band gap. To calculate the OE of LSCs containing GIRs, the FDTD method was used to modify the PDFs for reflection and transmission in the boundaries of

the LSC. Using this method, it is possible to optimize the pitch length of the GIR for the higher reflection of dye emission and calculate the reflection band gap of the GIR. To optimize PR pitch length, a dipole source radiating was considered with center frequency and line width of the dye emission spectrum. Afterwards, the ideal mirror pitch that is supposed to reflect the most dipole light into the waveguide was obtained. Lastly, the mirror band gap can be used to determine the improvement in sunlight absorption by dyes. In LSC, dyes are oriented randomly so that their overall radiation is incoherent and un-polarized as a result. It is required to perform three simulations in order to simulate an incoherent un-polarized dipole source. Each simulation considers a dipole that is orthogonal to the dipoles in the other simulations. After operation of each simulation, the fields can be added incoherently. In practice, this means that a dipole oriented along the x, y, and z axes was simulated, respectively, in each simulation with the intention of obtaining the un-polarized fields. As a final step, the results can be summed incoherently as follows [31]-[33]:

$$\langle |\mathbf{E}|^2 \rangle = \frac{1}{3} \left\{ |\mathbf{E}_{px}|^2 + |\mathbf{E}_{py}|^2 + |\mathbf{E}_{pz}|^2 \right\} \quad (6)$$

The quantity $\langle |\mathbf{E}|^2 \rangle$ refers to the time-averaged electric field intensity of an un-polarized dipole source, or a large number of randomly oriented dipoles in a spatial volume much smaller than the wavelength. For more understanding, an un-polarized dipole source was considered, which is created by a large number of incoherent dipole emitters contained in a small spatial volume that possess a random orientation. It can also be created by a single dipole that is randomly re-oriented every correlation time such that all possible orientations are equally sampled on time scales typical of photodetectors. To calculate the field distribution of an incoherent dipole, it is necessary to average over all possible dipole orientations. The incoherent electric field intensity at position \mathbf{r} is given by [32],[33]:

$$\langle |\mathbf{E}(\mathbf{r})|^2 \rangle = \frac{1}{4\pi} \int |\mathbf{E}(r, \theta, \varphi)|^2 \sin \theta d\theta d\varphi, \quad (7)$$

where $|\mathbf{E}(r, \theta, \varphi)|^2$ represents the electric field created at position \mathbf{r} by a dipole (at position \mathbf{r}_0) with an orientation given by the spherical angles θ and φ . A dipole of any orientation can be written as

$$\begin{aligned} \mathbf{p}(\theta, \varphi) = & \mathbf{p}\left(\frac{\pi}{2}, 0\right) \sin \theta \cos \varphi + \\ & + \mathbf{p}\left(\frac{\pi}{2}, \frac{\pi}{2}\right) \sin \theta \sin \varphi + \mathbf{p}(0,0) \cos \theta \end{aligned} \quad (8)$$

Since Maxwell's equations are linear, we can write the electric field from a dipole with orientation θ and φ as

$$\begin{aligned} \mathbf{E}(\theta, \varphi) = & \mathbf{E}\left(\mathbf{r}, \frac{\pi}{2}, 0\right) \sin \theta \cos \varphi + \\ & + \mathbf{E}\left(\mathbf{r}, \frac{\pi}{2}, \frac{\pi}{2}\right) \sin \theta \sin \varphi + \mathbf{E}(\mathbf{r}, 0,0) \cos \theta \end{aligned} \quad (9)$$

Substituting this into the Eq. 7 for the field intensity of an incoherent dipole gives

$$\begin{aligned} \langle |\mathbf{E}(\mathbf{r})|^2 \rangle = & \frac{1}{4\pi} \int \left| \mathbf{E}\left(\mathbf{r}, \frac{\pi}{2}, 0\right) \sin \theta \cos \varphi + \right. \\ & \left. + \mathbf{E}\left(\mathbf{r}, \frac{\pi}{2}, \frac{\pi}{2}\right) \sin \theta \sin \varphi + \right. \\ & \left. + \mathbf{E}(\mathbf{r}, 0,0) \cos \theta \right|^2 \sin \theta d\theta d\varphi \end{aligned} \quad (10)$$

In the end, we get

$$\begin{aligned} \langle |\mathbf{E}(\mathbf{r})|^2 \rangle = & \frac{1}{3} \left(\left| \mathbf{E}\left(\mathbf{r}, \frac{\pi}{2}, 0\right) \right|^2 + \left| \mathbf{E}\left(\mathbf{r}, \frac{\pi}{2}, \frac{\pi}{2}\right) \right|^2 + \right. \\ & \left. + \left| \mathbf{E}(\mathbf{r}, 0,0) \right|^2 \right). \end{aligned} \quad (11)$$

Therefore, the field distribution of an incoherent, un-polarized dipole is simply the average of the field distribution of three orthogonal dipoles. The same result can easily be shown for the magnetic field intensity or the Pointing vector.

The considered dye is $CH_3NH_3PbBr_3$ perovskite, the normalized absorption and emission spectra of which are shown in Fig. 2 [13]. The quantum efficiency of dye was considered to be 0.9 [13], the thickness of the edges to be 0.5 cm, equal to the smallest width of conventional silicon solar cells, and its surface dimensions to be 5 cm x 5 cm, the refractive index of the waveguide is 1.5 equal to the refractive index of PMMA. Ordinary (n_o) and extraordinary (n_e) refractive indices of the CLCs are 1.74 and 1.54,

respectively. All reflectors are assumed to have a right-handed structure.

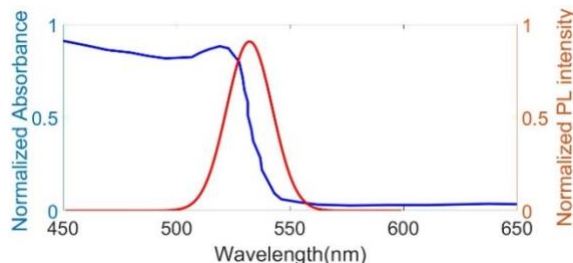


Fig. 2. Absorption (black curve) and emission (red curve) normalized spectra of $CH_3NH_3PbBr_3$ perovskite [13].

III. RESULTS AND DISCUSSION

In the first step, the OE of the LSC without mirrors was determined. To do this, some photons were sampled from air mass 1.5 and repeated the Monte-Carlo efficiency calculations. The error percentage in the results of the simulation decreased with an increase in the number of incident photons. It was found that the results remain the same for a sample of 10^6 photons, due to which all of the Monte-Carlo simulations that follow for 10^6 photons were carried out. Figure 3 (a) depicts the Monte-Carlo calculation of OE as a function of dye concentration. The maximum OE for the LSC is 7.659% at 0.03% wt. (optimal dye concentration). The spectral distribution of photons sampled from air mass 1.5 is shown in Fig. 3 (b), along with photons absorbed in LSC at the optimal concentration (0.03%). Furthermore, according to Beer-Lambert law, essential absorption occurs at wavelengths lower than 550 nm.

It is now possible to investigate the change in efficiency by placing a PR on the bottom side of LSC. To maximize dye radiation reflection into LSC, the optimal pitch length of the mirror was determined.

Figure 4 (a) displays the schematic representation of the simulation setup for this purpose. The present model involved an emitting dipole surrounded by a PMMA blade (LSC) and a PR at the bottom that reflects the dye radiation into the LSC. The dipole radiation spectrum was selected in accordance with the dye emission spectrum. The simulation was

conducted in three different polarization directions for the dipole, as explained in the previous section. It demonstrated the isotropic radiation of the dyes in the LSC. The calculation of the transmission in the current investigation was based on the fields adding to all three stages incoherently. A plot of transmission versus pitch length is presented in Fig. 4 (b). With a pitch length of 333 nm, the lowest transmission was achieved (highest reflection), 0.124, which decreased (increased) by 50% compared to the case without a mirror. Second- and third-order reflections were also evident that demonstrated insignificant efficiency.

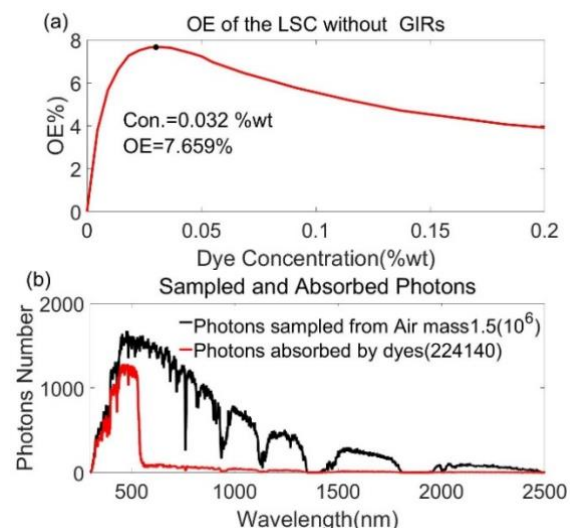


Fig. 3. (a) OE versus dye concentration for an LSC without a reflector. (b) Photon number versus wavelength for 10^6 incident photons sampled from Air mass 1.5 spectrum (black curve) and absorbed photons in LSC (red curve) for the optimal concentration illustrated with a black point in Fig. 4. (a).

According to Eq. 5, the pitch length required to reflect the central wavelength (530 nm) of the dye emission spectrum in the normal incident (where the GIRs' reflection band gap can overlap most of the dye emission spectrum) is 313 nm (black point on the curve shown in Fig. 4 (b)). There was, however, a shift of 20 nm towards longer pitches in the optimal pitch length (minimum of the curve shown in Fig. 4 (b), 333 nm). The reason for this shift was due to the reflection band of the mirror shifts towards the blue color as the angle of incidence increases. Mirrors can be designed by red-shifting the pitches, which compensates for the

blue-shifting of the reflection band. Figure 5 (a) shows the transmission spectra of the PR with the pitch lengths of 333 nm (black curve) and 313 nm (blue curve) curves in normal incidence for circularly polarized light and the dye emission spectrum (red curve).

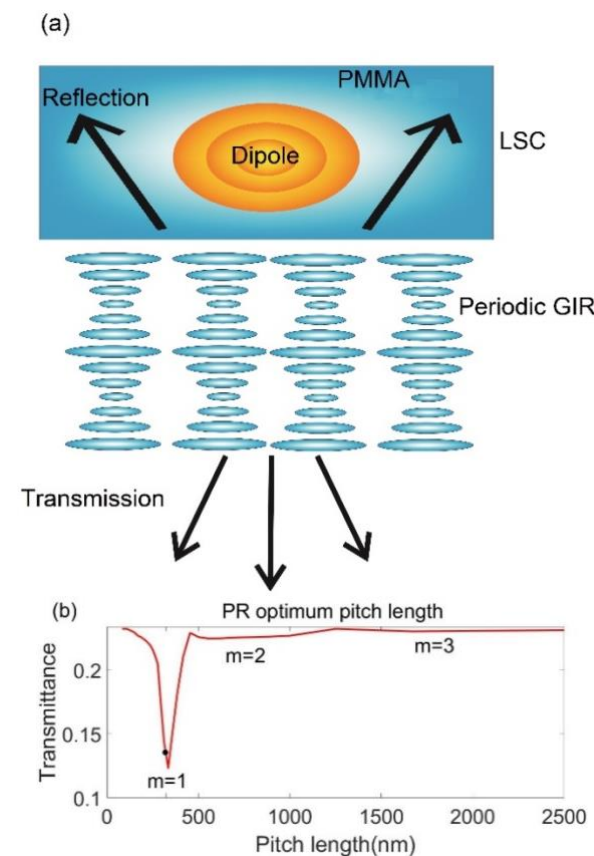


Fig. 4. (a) Schematic representation of simulation setup for transmission calculation of a dye embedded in LSC with a PR. (b) Un-polarized dipole transmission through a PR versus pitch length, dipole radiation wavelength is 530nm and FWHM 50nm corresponding with $CH_3NH_3PbBr_3$ dye fluorescence.

As shown in Fig. 4 (a), the 313nm pitch has a reflection band whose center is coincident with the dye emission band. On the other hand, the reflection band of the 333nm pitch has a shift that is about half the width of the dye emission spectrum towards long wavelengths. Figure 5 (b) illustrates the bandgap structure of a PR for $p=333$ nm and circularly polarized incident light. A dye emission band is shown by the distance between the white lines in this Fig. 4 (b). Due to the blue shift of the reflection band of the PR, with an increase in incident angle, the reflection band leaves the dye emission band after 25 degrees.

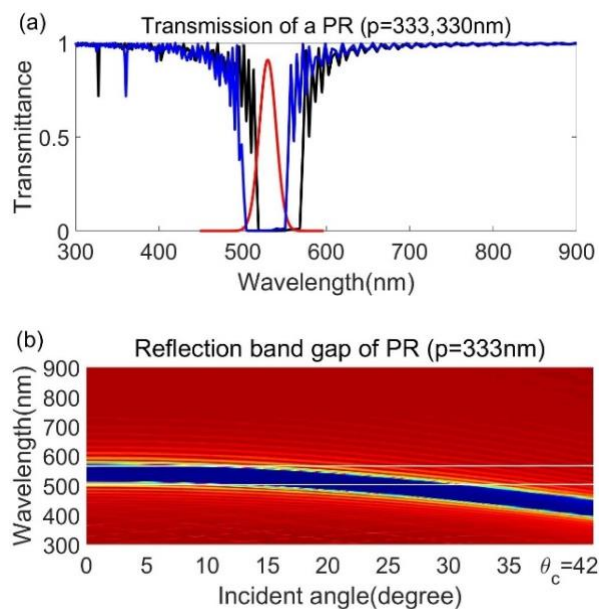


Fig. 5. (a) Dye emission spectrum (red curve) and transmission spectrum for a PR with $p=333$ nm (black curve) and $p=330$ nm (blue curve). (b) In the transmission band gap of a PR with a $p=333$ nm, white lines represent the dye emission edges.

It is obvious from Fig. 5 (b) that the escape cone is about 20 degrees, which demonstrates a decrease of 50% in comparison to the escape cone resulting from TIR ($\theta_c = \sin^{-1}\left(\frac{1}{n_{LSC}}\right) = 41.8^\circ$). This is completely in agreement with the current results in Fig. 4 (b). Additionally, the reflector can reflect the photons of sunlight that cannot be absorbed by dyes through the LSC. Thus, dyes will be given an additional chance to absorb sunlight, which will increase their absorption efficiency. a mirror band gap was utilized to calculate LSC's final absorption of sunlight. Incident photons that are not absorbed by the dyes can be reflected in the LSC if their wavelength is in the bandgap. As a result, their contribution was applied to the absorption rate in the Monte Carlo calculations.

Currently, having the input spectrum and the reflection coefficient from the boundaries, the final efficiency was calculated. Figure 6 (a) shows the changes in OE to concentration, the highest efficiency is 8.865% at a concentration of 0.03%wt which illustrates a 12% increase compared to the case without reflectors. We also see a decrease in the optimal concentration in the presence of the PR because the increase in absorption and reflection by the reflector leads to an increase in reabsorption (loss).

Followingly, the system tries to reduce the concentration to avoid high reabsorption losses. Figure 5 (b) displays that the reflection band deviates from the emission band for incident angles larger than 20 degrees, and the reflector cannot sweep the entire escape cone. Figure 6 (b) exposes the spectral distribution for the Photon number absorbed in LSC after reflection from the reflector. As it is evident, there is an extra absorption due to the reflection of light passing through the mirror.

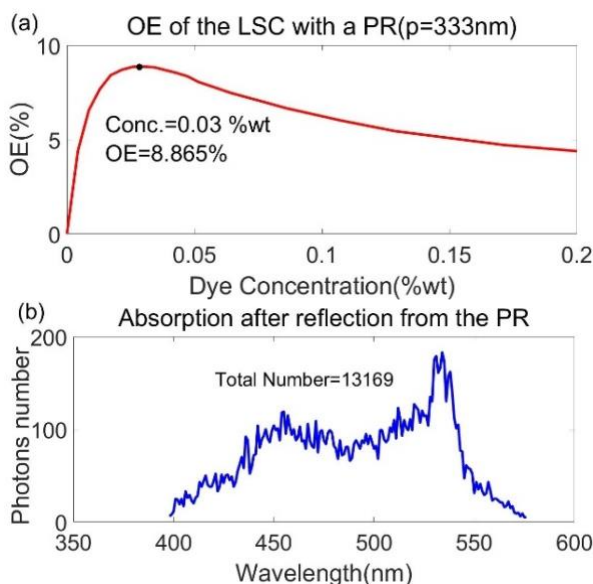


Fig. 6. (a) OE versus dye concentration of an LSC with a PR by $p=333\text{nm}$. (b) Photon number absorbed by dyes after reflection from the PR versus wavelength for dye concentration corresponded with the black point in Fig. 5. (a) (optimal concentration).

At this point, a QPR was considered with a refractive index that varies with a linearly variable spatial frequency according to Eq. 3 with $f_i = \frac{1}{p_i} = \frac{1}{450\text{nm}}$, $f_f = \frac{1}{p_f} = \frac{1}{270\text{nm}}$. Figure 7 (a) shows the experimental (black curve) [34] and simulation (red curve) results for the transmission spectrum of normal incident light for this QPR. There is a good agreement between the experimental and simulation results. The transmission band gap of the considered QPR is shown in Fig. 7 (b). Compared to the PR, it is apparent that the reflection bandwidth of the current reflecting device has increased significantly, allowing for full coverage of the escape cone.

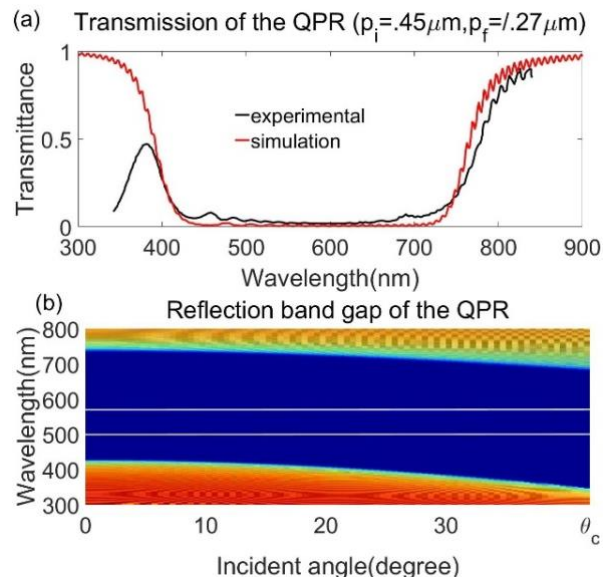


Fig. 7. a) experimental (black curve) [34] and simulation (red curve) result for transmission spectrum of normal incident light for a QPR with $f_i = \frac{1}{p_i} = \frac{1}{450\text{nm}}$, $f_f = \frac{1}{p_f} = \frac{1}{270\text{nm}}$. (b) In the reflection band gap of the QPR, white lines represent the dye emission edges.

Figure 8 (a) exhibits the variation of OE with dye concentration for an LSC with a QPR with $f_i = \frac{1}{435\text{nm}}$, $f_f = \frac{1}{303\text{nm}}$. In the case of the QPR, the optimal efficiency was 10.4% at a concentration of 0.028%, which represents an increase of 33% compared to the case without the reflector. The QPR also causes a higher decrease in optimal concentration than a PR because of the higher reflection and reabsorption. Figure 8 (b) shows the spectral distribution of the number of photons absorbed by LSC after reflection from the reflector.

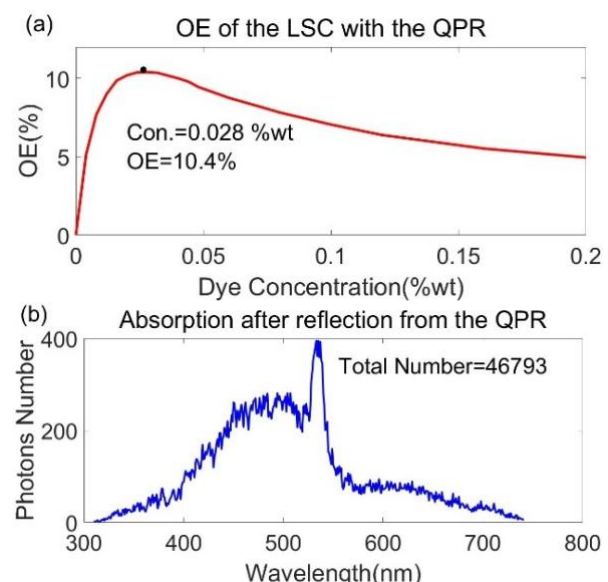


Fig. 8. (a) OE versus dye concentration of an LSC with the QPR. (b) The photon number absorbed in LSC after reflection from the QPR for dye concentration corresponded with the black point in Fig. 7. (a) (optimal concentration).

IV. CONCLUSION

The findings of the present results demonstrated that graded-index reflectors can significantly enhance the optical efficiency of luminescent solar concentrators (LSCs) by reducing escape cone loss and increasing sunlight absorption. With the periodic reflector (PR), the maximum efficiency increase was about 12%. The maximum improvement occurs once the center of the reflection band was shifted towards long wavelengths by 20 nm in comparison to the center of the dye emission spectrum. The efficiency improvement caused by PR was limited by the deviation of the reflection band from the dye emission band with increasing incident angle. Using quasi-periodic reflectors (QPRs) with a larger reflection band eliminated this limitation and showed a 33% efficiency improvement. In addition to decreasing the escape cone, reflectors can increase the absorption rate by reflecting transmitted photons into the LSC. A direct consequence of this was an increase in efficiency. In comparison to the PRs, QPRs demonstrated a significant improvement in absorption due to their larger bandwidth. Furthermore, the optimal concentration studies have revealed that by increasing the internal reflection in the presence of reflectors, the optimal concentration of the system declines.

REFERENCES

- [1] M. Okil, M.S. Salem, T.M. Abdolkader, and A. Shaker, "From crystalline to low-cost silicon-based solar cells: A review," *Silicon*, Vol. 14, pp. 1-17, 2021.
- [2] A.V. Rodrigues, D.A.R. de Souza, F.D.R. Garcia, and S.J.L. Ribeiro, "Renewable energy for a green future: Electricity produced from efficient luminescent solar concentrators," *Sol. Energy Adv.*, Vol. 2, pp.100013-100025, 2022.
- [3] M. Rafiee, S. Chandra, H. Ahmed, and S.J. Mc Cormack, "An overview of various configurations of Luminescent Solar Concentrators for photovoltaic applications," *Opt. Mater.*, Vol. 91, pp. 212-227, 2019.
- [4] M.G. Debije, M.P. Van, P.P. Verbunt, M.J. Kastelijn, R.H. van der Blom, D.J. Broer, and C.W. Bastiaansen, "Effect on the output of a luminescent solar concentrator on application of organic wavelength-selective mirrors," *Appl. Opt.*, Vol. 49, pp.745-751, 2010.
- [5] M. Collard, B. Racine, S. Meunier-Della-Gatta, D. Gross, B. Kerzabi, K. Millard, Y. Lee, A. Shum, O. Haeberlé, and C. Martinez, "Study of a liquid crystal impregnated diffraction grating for active waveguide addressing," In *Emerging Liq. Cryst. Technol. XVII*, Vol. 12023, pp. 1202302-1202310, 2022.
- [6] I. C. Khoo, *Liquid crystals*, John Wiley & Sons, 2022.
- [7] K. Miyagi and Y. Teramoto, "Construction of functional materials in various material forms from cellulosic cholesteric liquid crystals," *Nanomater.*, Vol. 11, pp. 2969-3119, 2021.
- [8] M. Belalia, C. Michel Mitov, A. Bourgerette, M. Krallafa, Belhakem, and D. Bormann, "Cholesteric liquid crystals with a helical pitch gradient: Spatial distribution of the concentration of chiral groups by Raman mapping in relation with the optical response and the microstructure," *Phys. Rev. E*, Vol. 74, pp. 051704-051712, 2006.
- [9] D.C. Zografopoulos, E.E. Kriezis, M. Mitov, and C. Binet, "Theoretical and experimental optical studies of cholesteric liquid crystal films with thermally induced pitch gradients," *Phys. Rev. E*, Vol. 73, pp. 061701-061711, 2006.
- [10] M. Mitov, "Polymer-cholesteric liquid-crystalline composites with a broad light reflection band," In *AIP Conference Proceedings*, Vol. 1736, pp. 020004-020010, 2016.
- [11] P. Yu, X. Chen, J. Gao, R. Yao, C. Ma, C. Zhang, H. Zhang, and Z. Miao, "Polymer-stabilized cholesteric liquid crystal films with broadband reflection formed by photomask polymerization," *Opt. Mater.*, Vol. 136, pp. 113385-113393, 2023.

- [12] E. Bagherzadeh-Khajehmarjan, A. Nikniazi, B. Olyaeefar, S. Ahmadi-Kandjani, and J.M. Nunzi, “Bulk luminescent solar concentrators based on organic-inorganic $\text{CH}_3\text{NH}_3\text{PbBr}_3$ perovskite fluorophores,” *Sol. Energy Mater. Sol. Cells*, Vol. 192, pp. 44-51, 2019.
- [13] E. Bagherzadeh-Khajehmarjan, S.M. Shakouri, A. Nikniazi, and S. Ahmadi-Kandjani, “Boosting the efficiency of luminescent solar concentrator devices based on $\text{CH}_3\text{NH}_3\text{PbBr}_3$ perovskite quantum dots via geometrical parameter engineering and plasmonic coupling,” *Org. Electron.*, Vol. 109, pp. 106629-10638, 2022.
- [14] S. Mirershadi and S. Ahmadi-Kandjani, “Efficient thin luminescent solar concentrator based on organometal halide perovskite,” *Dyes Pigm.*, Vol. 120, pp. 15-21, 2015.
- [15] Z. Pourali, B. Olyaeefar, S. Ahmadi-Kandjani, and A. Asgari, “Perovskite-coated window glasses as semi-transparent luminescent solar concentrators: an evaluation of different coating methods,” *J. Photonics Energy*, Vol. 11, pp. 027501-027501, 2021.
- [16] K. Nikolaïdou, S. Sarang, C. Hoffman, B. Mendewala, H. Ishihara, J.Q. Lu, B. Ilan, V. Tung, and S. Ghosh, “Hybrid perovskite thin films as highly efficient luminescent solar concentrators,” *Adv. Opt. Mater.*, Vol. 4, pp. 2126-2132. 2016.
- [17] H. Zhao, R. Sun, Z. Wang, K. Fu, X. Hu, and Y. Zhang, “Zero-dimensional perovskite nanocrystals for efficient luminescent solar concentrators,” *Adv. Funct. Mater.*, Vol. 29, pp. 1902262-1902270, 2019.
- [18] H. Zhao, Y. Zhou, D. Benetti, D. Ma, and F. Rosei, “Perovskite quantum dots integrated in large-area luminescent solar concentrators,” *Nano energy*, Vol. 37, pp. 214-223, 2017.
- [19] Z. Zheng, Y. Zhang, X. Cao, G. Gu, Y. Tian, and X. Zhang, “Modeling and comparison of bulk and thin-film luminescent solar concentrators based on colloidal perovskite quantum dots,” *Opt. Lett.*, Vol. 47, pp. 4367-4370, 2022.
- [20] D.K. Hwang and A.D. Rey, “Computational modeling of the propagation of light through liquid crystals containing twist disclinations based on the finite-difference time-domain method,” *Appl. Opt.*, Vol. 44, pp. 4513-4522, 2005.
- [21] V. Ilyina, S.J. Cox, and T.J. Sluckin, “FDTD method for light interaction with liquid crystals,” *Mol. Cryst. Liq. Cryst.*, Vol. 422, pp. 1-10, 2004.
- [22] J. Shu, X. Zhang, P. Wang, R. Chen, H. Zhang, D. Li, P. Zhang, and J. Xu, “Monte-Carlo simulations of optical efficiency in luminescent solar concentrators based on all-inorganic perovskite quantum dots,” *Physica B*, Vol. 548, pp. 53-57, 2018.
- [23] A. Mouldi and M. Kanzari, “Design of an omnidirectional mirror using one-dimensional photonic crystal with graded geometric layers thicknesses,” *Optik*, Vol. 123, pp. 125-131, 2012.
- [24] R. Zohrabi and A. Namdar, “Perfect tunable all-optical diode based on periodic photonic crystal grand graded structures,” *J. Opt. Commun.*, Vol. 40, pp. 187-193, 2019.
- [25] C. Bosshard, J. Hulliger, M. Florsheimer, and P. Gunter, *Organic nonlinear optical materials*, CRC Press, 2001.
- [26] F.V. Ignatovich and V.K. Ignatovich, “Optics of anisotropic media,” *Phys. Usp.*, Vol. 55, pp. 709-721, 2012.
- [27] T. Irvine, “Sine Sweep Frequency Parameters,” 1998.
- [28] R. Dreher, G. Meier, and A. Saupe, “Selective reflection by cholesteric liquid crystals,” *Mol. Cryst. Liq. Cryst.*, Vol. 13, pp. 17-26, 1971.
- [29] D.K. de Boer, D.J. Broer, M.G. Debije, W. Keur, A. Meijerink, C.R. Ronda, and P.P. Verbunt, “Progress in phosphors and filters for luminescent solar concentrators,” *Opt. Express*, Vol. 20, pp. A 395-A405, 2012.
- [30] M. Cao, X. Zhao, and X. Gong, “Achieving high-efficiency large-area luminescent solar concentrators,” *J. Amer. Chem. Soc. Au*, Vol. 3, pp. 25-35, 2023.
- [31] W. Demtröder, *Laser spectroscopy: Basic concepts and instrumentation*, Springer, 1985.
- [32] G.R. Fowles, *Introduction to modern optics*, Dover Publications, 1989.

[33] L. Novotny and B. Hecht, *Principles of nano-optics*, Cambridge University Press, 1989.

[34] D.J. Broer, J. Lub, and G.N. Mol, “Wide-band reflective polarizers from cholesteric polymer networks with a pitch gradient,” *Nature*, Vol. 378, pp. 467-469, 1995.



Ramin Zohrabi was born in Miandoab, Iran, in 1989. He received his BSc degree in atomic and molecular physics from Urmia University, Urmia, Iran in 2012 and MSc degree in optics and laser physics from the University of Tabriz, Tabriz, Iran, in 2015. He joined the Physics Department of the University of Tabriz as a PhD candidate in atomic and molecular physics in 2018.

His current research activities are in the fields of luminescent solar concentrators, nonlinear optics, photonic crystals and liquid crystals, optical properties of graded index materials, plasmonic, and fluorescence enhancement.



Abdolrahman Namdar was born in Tabriz, Iran, in 1961. He received his MSc degree in atomic and molecular physics and a PhD degree in laser physics from the University of Tabriz, Tabriz, Iran. He is a professor of physics in the Physics Department of the University of Tabriz. His current research activities are in the fields of nonlinear optics, photonic crystals, metamaterials, graphene, and nano-photonics. Prof. Abdolrahman Namdar has authored and co-authored more than 79 scientific papers in peer-reviewed international journals.



Sohrab Ahmadi-Kandjani was born in Tabriz, Iran. He received his MSc degree in atomic and molecular physics from the University of Tabriz, Tabriz, Iran, in 1998 and a PhD degree in physics from the University of Angers, Angers, France in 2007. He is a professor of physics in the Physics Department of the University of Tabriz.

His current research activities are in the fields of optical biosensors, luminescent solar concentrators, computational ghost imaging, optoelectronic devices, and nonlinear optical properties of materials. Prof. Sohrab Ahmadi-Kandjani has authored and co-authored more than 125 scientific papers in peer-reviewed international journals.



Babak Olyaeefar was born in Tabriz, Iran. He received his PhD degree in photonics from the University of Tabriz, Tabriz, Iran in 2015. He joined the Physics Department of the University of Tabriz as a Postdoctoral Fellow from 2016 to 2021. He is now a Postdoctoral Researcher at UNAM-Institute of Materials Science and Nanotechnology at Bilkent University, Ankara, Turkey.

His current research activities are in the fields of diode lasers, solar energy conversion, and plasmonic, and liquid crystals. Dr. Babak Olyaeefar has authored and co-authored more than 23 scientific papers in peer-reviewed international journals.